Evidence of high-K isomerism in $_{102}^{256}$No$_{154}$

K. Kessaci [1] B. J. P. Gall [1,*] O. Dorvaux,[1] A. Lopez-Martens [2] R. Chakma,[2] K. Hauschild [2] M. L. Chelnokov,[3]
V. I. Chepigin,[3] M. Forge [1] A. V. Isaev [3] I. N. Izosimov,[3] D. E. Katrasev,[3] A. A. Kuznetsova,[3] O. N. Malyshev [3]
R. Mukhin,[3] J. Piot [4] A. G. Popeko [3] Yu. A. Popov,[3] E. A. Sokol,[3] A. I. Svirikhin [3]
M. S. Tezekbayev,[3,5] and A. V. Yeremin [3]

[1]*Université de Strasbourg, CNRS, IPHC UMR 7178, 67037 Strasbourg, France*
[2]*IJCLab, IN2P3-CNRS, Université Paris Saclay, 91400 Orsay, France*
[3]*Flerov Laboratory of Nuclear Reactions, JINR, 141 980 Dubna, Russia*
[4]*Grand Accélérateur National d'Ions Lourds, CEA/DSM-CNRS/IN2P3, Caen, France*
[5]*The Institute of Nuclear Physics, 050032 Almaty, The Republic of Kazakhstan*

Isomeric states in ^{256}No were investigated using internal conversion electron and γ-ray spectroscopy with the GABRIELA detection system at the focal plane of the SHELS recoil separator, at the Flerov Laboratory for Nuclear Research (FLNR, JINR, Dubna). The nuclei of interest were produced using the highly asymmetric fusion-evaporation reaction ^{238}U(^{22}Ne, $4n$) ^{256}No. The emission of internal conversion electrons and γ rays occurring between a ^{256}No implantation and a subsequent α-decay event were studied, resulting in the observation of high-K isomerism in this nobelium isotope. The nature of the isomeric states is discussed in terms of possible two- and four-quasiparticle structures.

I. INTRODUCTION

The ^{256}No isotope was first studied in 1963 by Donets *et al.* [1,2] using the ^{238}U(^{22}Ne, $4n$) ^{256}No highly asymmetric fusion reaction. As compared to the ^{48}Ca induced reactions on lead targets, this reaction enables the production of more neutron-rich nobelium isotopes even if the higher heat of the reaction increases the number of evaporated neutrons. With a 3.4 ± 0.3 μb cross section [3], the ^{208}Pb(^{48}Ca, $2n$) ^{254}No reaction was widely used for prompt and decay spectroscopy studies (see [4] and references therein). Ground state rotational bands (GSB) were observed in this nucleus and its neighboring ones. High-K isomerism was also established in these deformed nuclei. A trial of ^{256}No study using a ^{48}Ca beam impinging on a radioactive ^{210}Pb was attempted with our setup a few years ago, but faced target purity issues.

Both highly asymmetric reactions on actinide target and reactions based on doubly magic target and/or beam were conducted for spectroscopy of very heavy elements as well as for the quest of the heaviest elements. The use of targets around doubly magic ^{208}Pb associated with heavier and heavier beams was pushed to its limits with the synthesis of new superheavy elements (SHE) up to copernicium [5] and nihonium ($Z = 113$) [6–8]. Heavier SHE up to $Z = 118$ [9,10] were synthesized by fusion-evaporation reactions using the doubly magic ^{48}Ca beam impinging on heavier and heavier targets up to ^{249,251}Cf [11]. Beyond the proof of existence

of these chemical elements, these studies also addressed the question of the existence of an ultimate proton magic number leading to a hypothetical "island of stability" with long-lived superheavy elements [12].

For such heavy elements, theoretical models are at their limits. Their predictions do not agree on the single-particle structure around nobelium isotopes and on the position of an ultimate island of stability [13–15]. A sort of consensus emerged placing this island at a proton number of 114. The optimal neutron number is still controversial, but definitely higher than the heaviest observed flerovium isotope (^{289}Fl). More neutron-rich isotopes might also be synthesized in the future through deep inelastic reactions involving actinide targets and projectiles [16]. Similarly, detailed studies of more neutron-rich nobelium nuclei are needed to gather precise information on the excitation energy and ordering of neutron and proton single-particle states for very heavy elements. To produce these nuclei one can take advantage of the neutron richness of targets like uranium, plutonium, and heavier actinides, leading to very asymmetric fusion-evaporation reactions. Although these highly asymmetric fusion reactions are rather well known, it took many years of experimental developments to enable the present study. Researchers at the GSI have successfully synthesized ^{256}No using ^{22}Ne $+$ ^{238}U although their statistics enabled only the measurement of the ground state lifetime and associated α-decay energy [17]. Decay spectroscopy of ^{256}No was also attempted in 2006 at the University of Jyväskylä using the RITU gas-filled separator [18] together with the JUROGAM [19] spectrometer around its target position and the GREAT [20] detector at the focal plane [21]. Unfortunately, the ^{22}Ne beam impinging on

^{238}U target induces very slow recoiling nobelium nuclei. The kinetic energy loss and straggling into the low-pressure RITU helium gas and in the thin mylar foil—that enables the silicon array to operate in vacuum—prevented these nuclei from reaching the focal plane implantation detector [22]. Finally, the first in-flight study of excited states in ^{256}No could be performed at the FLNR almost 60 years after Donets using the same reaction. This study is very challenging from several points of view since ^{256}No is one of the most proton rich nuclei with $N = 154$ neutrons ever studied in α-γ-e$^-$ spectroscopy. In this paper, evidence for high-K isomerism is reported in ^{256}No. The corresponding lifetime and energy measurement are detailed and different decay scenarios are discussed.

II. EXPERIMENTAL FEATURES

The ^{256}No nuclei were produced through the ^{238}U(^{22}Ne, $4n$) ^{256}No highly asymmetric fusion-evaporation reaction at the Flerov Laboratory for Nuclear Research (FLNR, JINR, Dubna). The ^{22}Ne beam was provided by the U400 cyclotron with intensities ranging between 600 pnA and 1 p μA for mid-target energies of 113 and 116 MeV. The 99,99% pure ^{238}U target was deposited on a 1.5 μm titanium backing and mounted on a rotating wheel frame. The evaporation residues (ERs) were separated from other recoiling nuclei by the Super Heavy ELements Separator (SHELS) [23,24]. The fact that uranium had the U_3O_8 oxide chemical form reduced the recoil transmission for the experiment.

The GABRIELA [25] precision spectroscopy setup is composed of a modular time of flight (ToF) system [26], a double-sided silicon strip implantation detector (DSSD) with 128×128 strips leading to 16 384 pixels preceded by eight silicon strip detectors (16×16 strips each where only the strips facing the DSSD are used) in a tunnel configuration, all surrounded by five high-purity Compton-suppressed germanium (HPGe) detectors. The HPGe detector right behind the DSSD is the CLODETTE [27] clover detector inserted in an active Compton suppression shield based on bismuth germanate (BGO) crystals. For this HPGe detector, "add-back" summation is performed when two adjacent crystals are hit in coincidence. The four lateral HPGe detectors behind the eight silicon tunnel detectors are single large-volume Ge crystals surrounded by individual anti-Compton BGO shields. The Compton suppression was done via a bit marker associated with the HPGe energy events in the data rather than through hardware suppression. The compact geometry ensures an optimal detection efficiency (see [25,28]). Data were recorded in a total data readout mode associating each individual analog-to-digital converter (ADC) readout to a timestamp with a 1 μs clock. This experiment was performed in a beam-on/beam-off mode, with a 4.0 ms active cycle (beam on) followed by a 1.4 ms passive decay time (beam off).

To maximize the transmission of nobelium ions, the first emissive foil of the ToF detector was removed. Only the ToF module closest to the DSSD was used for this experiment. For the same reason, no degrader foil could be used to reduce the background of the scattered beam in the DSSD. As a consequence, the implantation DSSD thresholds had to be set

higher than usual with GABRIELA, to ≈ 120 keV on the back strips and to ≈ 100 keV on the front ones.

Acting as a velocity filter, SHELS was optimized for transportation of slow ERs. This experiment was its first operation in this very asymmetric mode. A 6.5% transmission was previously measured [24] for the ^{22}Ne + ^{197}Au reaction.

For this experiment, the strips of the DSSD were calibrated using the α and internal conversion electron (ICE) signals generated by ERs implanted in the DSSD and produced in the ^{198}Pt(^{22}Ne, xn) $^{220-x}$Ra reaction. The HPGe detectors were calibrated using the γ rays from standard ^{152}Eu and ^{133}Ba sources first and the in-beam calibration was verified with the decay from known isomers in ^{215}Ra [29]. Calibration of the tunnel detector strips was performed using the isomeric ICE emissions of implanted ^{214}Ra [30] selected by gates on the γ rays in coincidence.

To search for genetic decay correlations spanning many orders of magnitude in time, radioactive decays are transformed into a logarithmic base 2 timescale and plotted according to their corresponding decay energies, as originally proposed by Bartsch *et al.* [31]. Such a transformation has allowed the discovery by the GABRIELA Collaboration of isomeric states in ^{253}No [32] and ^{255}Lr [33].

For states with half-lives shorter than 500 μs, the radioactive decay signal in the implantation DSSD occurs on the tail of the implantation signal leading to a distorted energy measurement. As described in [34] and illustrated in Fig. 3 of the same reference, a time-dependent correction of the measured decay signal amplitude was performed for decay events occurring within 500 μs of an implantation signal. However, no correction could be applied to decays occurring less than 9 μs after the recoil due to lack of calibration data, so the energies of such decays cannot be used in the data analysis.

III. EXPERIMENTAL RESULTS

The α decays are isolated through a position-correlated search of the implantation of an ER followed by a decay signal in the same pixel. The $\log_2$ plot for the ^{256}No is presented on Fig. 1. Due to a high counting rate in the implantation DSSD, the random correlations starting around 8 s (2^{23} μs) appears clearly in this figure. While the distribution of the α measured in the decay of ^{215}Ra is well separated from the random correlations at $\log_2(T_\alpha - T_{\text{Recoil}} [\mu s])$ less than 15, this is not the case for ^{256}No with a published half-life of 2.91 ± 0.05 s [17]. Note that we see appearing at 8699 keV some ^{215}Ra decays produced on some ^{198}Pt impurities in the target. Considering the cross section of this ^{198}Pt(^{22}Ne, xn) $^{220-x}$Ra reaction and the low number of ^{215}Ra observed, the impurity level is less than 100 ppm.

An energy of 8437 ± 10 keV was extracted by a skewed-Gaussian fit on a background subtracted spectrum for the ^{256}No ground state α decay. Since the energy calibration was obtained from radium α decay peaks, a kinematical correction was applied to account for the difference in recoiling daughter energies [35], ^{256}No being 20% heavier than the radium reference isotopes. This effect introduces a 7 keV shift leading to an 8444 ± 10 keV α decay energy for ^{256}No. This value
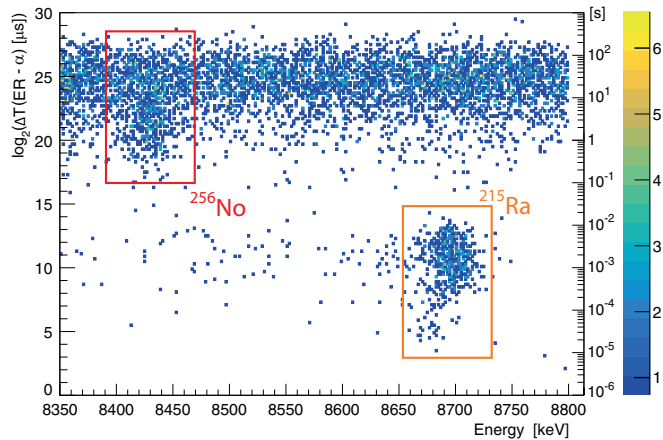
FIG. 1. Logarithmic plot of the time difference between position-correlated α and ER as a function of α energy. Random correlations are spread over the whole energy range around $\log_2(\Delta T [\mu s]) \simeq 25$. The right scale enables direct reading in seconds. The ^{256}No and ^{215}Ra ground state α-decay events are located by squares.

is in good agreement with high-resolution measurements of Asai *et al.* [36].

As can be seen in Fig. 1, the half-life of ^{256}No is close to the distribution of the random correlations. Therefore, an estimation of the total number of nobelium nuclei observed was extracted for data with the beam-off marker. Under these conditions, a total of 96 ± 2 ^{256}No ground state decays are observed and isolated from random correlations. A $74.5 \pm 4.9\%$ duty cycle was measured in similar conditions with ^{215}Ra. Accounting for a 50% detection efficiency, one can estimate that that a total of 753 ± 36 ^{256}No arrived in the focal plane of GABRIELA.

In order to measure the lifetime of ^{256}No, a projection of the data in Fig. 1 on the time axis was made with an energy gate of 8400–8460 keV (Fig. 2). To separate the ^{256}No from the random correlations, a two-component fit was used. A half-life of 2.77 ± 0.24 s was extracted, in good agreement with literature [2,17].

Isomeric states in ^{256}No were searched for using the calorimetric method [37]. When an isomeric state is implanted in the DSSD, typically the next signal observed in the same pixel is the electron shower (summation of internal conversion electrons, Auger electrons, X rays, etc.) detected due to the decay of the isomer. The subsequent α decay of the ER will also occur in the same pixel, thus, detecting position and time correlated ER-e-α sequences provides direct evidence of isomeric decays. Figure 3 shows the logarithmic time difference between an ER and the subsequent event in the same pixel as a function of the second generation energy. Isomeric decay events clearly appear at the α-decay energies of ^{256}No and ^{215}Ra. In the 8410–8450 keV energy range used for the ^{256}No selection, 14 ER-e-α delayed coincidences were observed within a few μs of the recoil signal in the same pixel. Due to the lower detection threshold on the DSSD backside strips, one additional event was established requiring these temporal correlations on the basis of strips only. Similarly, around 8700 keV we can see the well-known 7 μs isomeric state in ^{215}Ra,
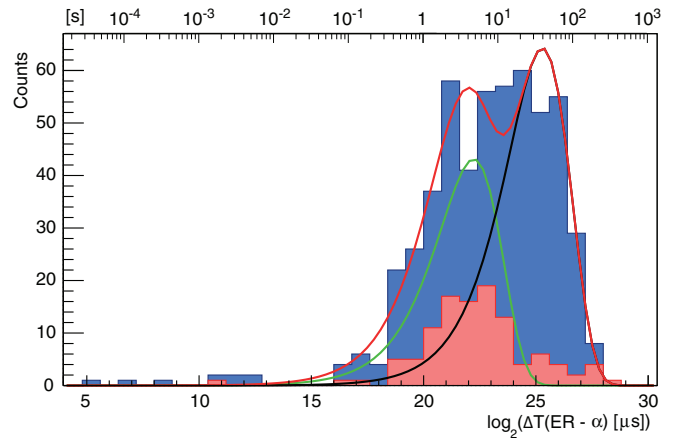

FIG. 2. Logarithmic time difference distribution extracted from Fig. 1 with an α energy gate between 8410 and 8460 keV. The distribution obtained with the beam-on condition is displayed in blue and the distribution obtained out of beam is displayed in red. The half-life of ^{256}No is extracted via multicomponent fit to separate the nobelium contribution (green) from the random correlations (black). The top scale enables direct reading in seconds.

resulting from reactions with ^{198}Pt impurities in the target. The inset of Fig. 3 shows the decay time of these 15 isomeric decays with respect to their energies. As explained earlier, the energies of events occurring within less than 9 μs (red dashed line) from the recoil implant are overestimated. Therefore, only their decay time can be considered for the interpretation. The energy distribution of the nine non piled-up data points ranges between 130 and 520 keV. The statistics is unfortunately too low to draw more conclusions.
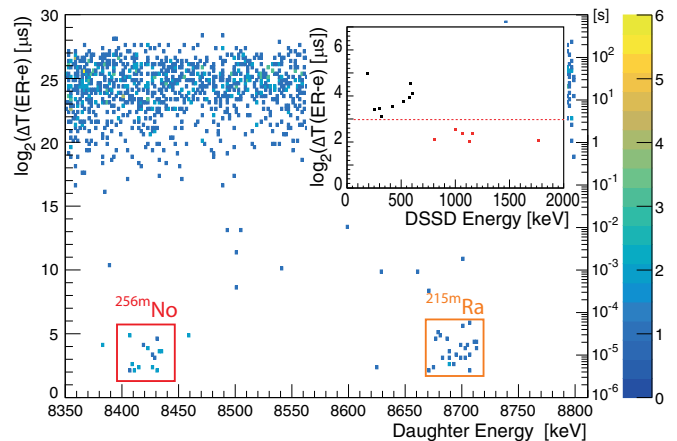
FIG. 3. Logarithmic plot of the time difference between the implantation of a recoil and the first generation decay that occurs in the same pixel as a function of the energy of the second generation decay. The right scale enables direct reading in seconds. The events corresponding to the isomeric decay of ^{256m}No and ^{215m}Ra are shown by the red squares. The inset displays the same logarithmic time plot for the 15 ^{256m}No events, this time as a function of their energy. Events with time difference long enough to enable pileup correction are displayed in black. Energies of the ICE in red are not relevant.

FIG. 4. Logarithmic time difference distribution extracted from Fig. 3 with an α energy gate between 8400 and 8460 keV. The Lifetime of ^{256m}No is extracted from these points (see text for details). Top scale enables direct reading in microseconds.
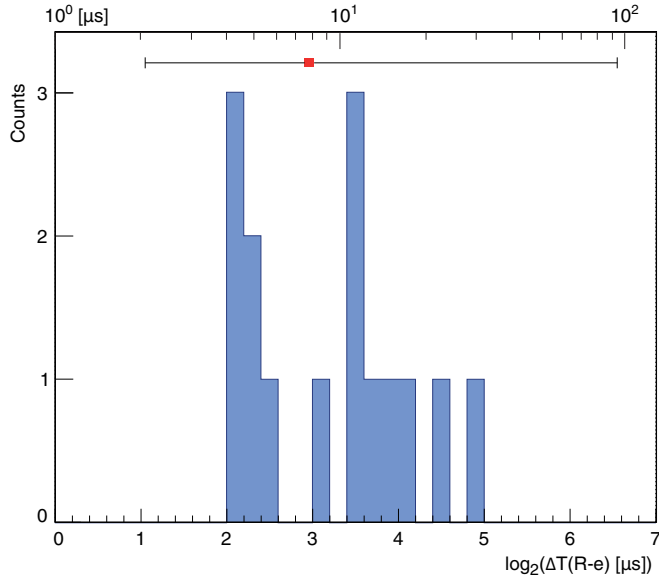
Assuming that the 15 events displayed in Fig. 4 correspond to the decay of the same ^{256m}No isomer, a half-life of $7.8^{+8.3}_{-2.6}$ μs was determined by means of the method developed by Schmidt for low statistics measurements [38]. The corresponding lifetime was overlaid to the data on top of Fig. 4. It is important to underline here that the fastest contribution to this time distribution is truncated due to electronics dead time and that 6 events out of 15 are packed at the shortest edge of the measurement window (Fig. 4). One may thus also consider that the observed distribution results from two isomers. Applying the Schmidt method to the nine slowest data points gives a half-life of $10.9^{+21.7}_{-4.3}$ μs and an upper limit of 6 μs can be given for the partially observed fast isomer. A higher statistics experiment with digital electronics is definitely needed in order to clarify this situation.

A search for γ rays in coincidence with these 15 isomeric events was performed, and 13 γ rays could be associated to the decay of ^{256m}No. The γ-DSSD correlations are shown in Table I associated together with coincident tunnel events and the sum energy. Among these 13 γ rays, 5 of them have energies corresponding to nobelium x rays (L at 23/27 keV and K at 127 keV). It is important to underline that out of these 15 isomeric decays observed in the DSSD, 13 were observed in coincidence with a signal in the tunnel detectors. No specific structure appeared in the DSSD-tunnel or HPGe-tunnel two-dimensional histograms. All these events were therefore reported in Table I, where the total energy in coincidence is reconstructed for each event. Unfortunately, such scarce statistics does not allow for definitive conclusions. Nevertheless, these data enable a lower limit of 1089 keV for the excitation energy of this (these) ^{256m}No new isomeric state(s) to be set.

TABLE I. List of γ rays, low energy electron showers (DSSD) and ICE energies (tunnel) in coincidence for the 15 observed isomeric decays of ^{256m}No. One can note that some of the γ rays have energies corresponding to nobelium x rays (L at 23/27 keV and K at 127 keV). The γ-ray energy marked with "AB" is a sum of two γ rays observed in coincidence in two crystals of the clover detector (add-back mode) [39]. When two nonneighboring crystals of clover or two strips of tunnel detectors are hit in coincidence, the energies are indicated as recorded in parallel (28 ∥ 537). The DSSD events marked with "PU" have a lifetime below the pileup correction threshold and should not be considered (no sum was calculated). Errors bars were estimated accounting for the variances from fits on the DSSD (11 keV) and the tunnel (17 keV) detectors' spectra. Although the HPGe variances are energy dependant, their contribution to the errors bars are almost neglectable with respect to the Si detectors.

DSSD energy (keV)	Tunnel energy (keV)	HPGe energy (keV)	Sum (keV)
187			187 ± 26
254	101	27	382 ± 48
421	63		484 ± 48
518	121		639 ± 48
303	101	28 ∥ 537	969 ± 48
318	73 ∥ 139	463^{AB}	993 ± 62
576	91	127 ∥ 205	999 ± 48
589	91 ∥ 98	255	1033 ± 62
604	92 ∥ 154 ∥ 216	23	1089 ± 74
809^{PU}	86	133	
999^{PU}	139	127	
1063^{PU}	64 ∥ 163	372^{AB}	
1131^{PU}		307	
1154^{PU}	28	382	
1768^{PU}		0	

IV. DISCUSSION

A schematic drawing of the single-particles states around the neutron and proton Fermi levels in ^{256}No is presented in Fig. 5. Potential particle-hole excitations across the Fermi level are represented by arrows. Due to the residual spin-spin interaction between quasiparticles, all these two-quasiparticle (2-qp) states can lead to two coupling schemes, the "Gallagher favored" being slightly lower in energy than the unfavored one [42,43]. On the proton side, one should highlight the presence of three 2-qp favored states, the $K^\pi = 3^+$, 5^-, and 8^- states, for the discussion of the possible lower lying proton high-K isomer, the other ones being higher in energy. They correspond respectively to the favored $\pi^2\{[521]\frac{1}{2}^- \otimes [514]\frac{7}{2}^-\}_{3^+}$, $\pi^2\{[624]\frac{9}{2}^+ \otimes [521]\frac{1}{2}^-\}_{5^-}$, and $\pi^2\{[624]\frac{9}{2}^+ \otimes [514]\frac{7}{2}^-\}_{8^-}$ two-quasiproton configurations. This excitation scheme is observed in the closest known even-even isotope ^{254}No, where a $\approx$1.3 MeV 8^- state decays to the GSB mainly via an intermediate 3^+ structure at $\approx$ 1 MeV excitation energy [44–47]. It is worth pointing out, however, that the nature of the 8^- state in ^{254}No is still under debate.

On the neutron side, the lowest lying states should be the $K = 2^+$, 5^-, and 7^- states originating from the favored coupling of the $\nu^2\{[622]\frac{3}{2}^+ \otimes [620]\frac{1}{2}^+\}_{2^+}$,
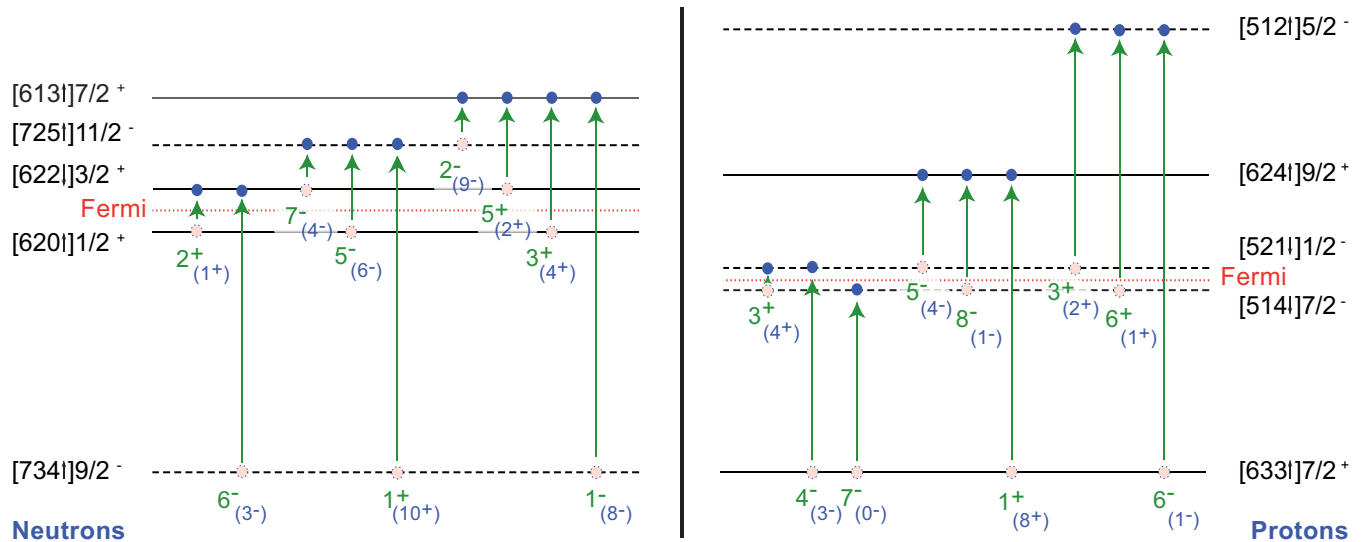
FIG. 5. Illustration of the possible two quasiparticles states on a neutron and proton single-particle scheme based on known experimental sequences of states in neighboring isotones and isotopes. The sequence was adapted from [40] where only the $[622]\frac{3}{2}^+$, $[613]\frac{7}{2}^+$, and $[725]\frac{11}{2}^-$ were exchanged with respect to the order established in the case of ^{256}Rf to be coherent with observations [41], these single-particle states are very likely to be rather close in energy. For two-quasiparticle excited states, K value and parity are indicated in green (blue within brackets) for the favored (resp. unfavored) Gallagher [42,43] combination. Spin orientation is indicated by an arrow in the Nilsson labeling of a single nucleon orbital in order to facilitate application of Gallagher rules.

$\nu^2\{[725]\frac{11}{2}^- \otimes [620]\frac{1}{2}^+\}_{5^-}$, and $\nu^2\{[725]\frac{11}{2}^- \otimes [622]\frac{3}{2}^+\}_{7^-}$ two-quasineutron configurations. At variance with ^{254}No, which has the Fermi level in the $N = 152$ gap, smaller excitation energies are expected for this state in ^{256}No with respect to the one observed in ^{254}No. By construction, one expects a very small energy difference between the $_{\nu^2}5^-$ and $_{\nu^2}7^-$ 2-qp states, both having a rather limited excitation energy with respect to the $_{\nu^2}2^+$. Therefore, both these high-K states are expected to decay directly to the GSB.

High-K isomerism results from the forbiddenness of γ-ray transitions when the difference in K—the projection of the total angular momentum J on the deformation axis—differs by more units than the multipolarity of the electromagnetic transition. The systematics of high-K isomer decays from Löbner [48] compiles the observed hindrance factor with respect to the Weisskopf estimates of electromagnetic transitions half-lives [49] as a function of multipolarity and electric or magnetic character of the isomer decay transition. A more recent review by Kondev *et al.* [50] updates these systematics for nuclei with $A > 100$ with improved description of $E1$, $E2$, and M1 transitions. Both these systematics enable a rough estimation of the expected half-lives for potential high-K isomer-decay scenarios.

Considering the 2-qp states discussed above ($_{\pi^2}3^+$, $_{\pi^2}5^-$, and $_{\pi^2}8^-$ for protons and $_{\nu^2}2^+$, $_{\nu^2}5^-$, and $_{\nu^2}7^-$ for neutrons), both the proton and the neutron first 2-qp states have rather low K. Thus, the decay form these bandheads to the $K^\pi = 0^+$ GSB will imply very low hindrances that cannot account for the observed isomer lifetime(s). At the same time, the presence of these $_{\nu^2}2^+$ and $_{\pi^2}3^+$ low-K band structures offers an accelerated decay path for potential medium K bandheads.

As is the case in ^{254}No [44–47], the $_{\pi^2}5^-$ state is not expected to be isomeric. The decay of the $_{\pi^2}8^-$ is known to be hundreds of milliseconds in ^{254}No [44–47] and can neither account for the measured ^{256m}No half-life nor correspond to the ^{256m}No observed half-life nor explain the observed spectra. The current data therefore suggest that the 7^- and possibly the 5^- and 2^- quasineutron excitations must lie below the 8^- two-quasiproton state and that they are responsible for the isomerism in ^{256}No. The isomeric decays would involve high-energy $E1$ transitions to either the 8^+ and 6^+ or 6^+ and 4^+ members of the GSB, followed by highly converted $E2$ transitions within the band. According to the high-K isomer systematics by Kondev *et al.* [50], such decays would have microsecond lifetimes. Regarding energetics, the decay of the 7^- two-quasineutron state would explain the large range of detected energies, with a possible contribution from the 5^- state at lower energies.

From the 15 observed isomeric transitions associated with the 753 ± 36 ^{256}No implanted in the DSSD, and accounting for detection efficiency, one finds a ratio between observed isomeric decays and ground state decays of $\approx$4%. Both such a low value and the observed energy distribution are rather typical for a 4-qp isomer. Isomers built on 2-qp configurations usually gather up to 15–20% of the total isomeric decay flux. For our total number of implanted ^{256}No, this should correspond to 50–75 observed decays. Given the high thresholds and electronics dead time, the fastest decays and those corresponding to small energy depositions in the DSSD go undetected, which could explain the low isomeric ratio. One could imagine that the unobserved 2-qp decays occur through a decay path with ICE sums below our 100 keV detection

threshold or through an isomer fast enough to be at the edge of our observation limits, as Fig. 4 seems to indicate.

V. CONCLUSION

This experiment has given the first evidence of at least one high-K isomer in ^{256}No. Assuming a single isomer, a half-life was measured ($t_{1/2} = 7.8^{+8.3}_{-2.6}$ μs) and a lower limit of 1089 keV was deduced for the excitation energy of this state. Possible interpretation in terms of two-quasiparticle states ws discussed, highlighting the probable role of both the $_{\nu^2}7^-$ and $_{\nu^2}5^-$ states. The isomeric ratio indicates that a significant part of the decay path has been missed. An unambiguous discussion about isomeric ratios can only be drawn on the basis of a decay scheme. To conclude on the nature of the observed isomer(s), it is definitely needed to repeat this experiment with lower threshold (below 70 keV) and faster acquisition based on digital electronics where fast pileup can be decorrelated using digital trace analysis. Such an experiment is mandatory to establish the correct interpretation and give more detailed spectroscopic information for nobelium isotopes in this unknown region above the $N = 152$ neutron gap.

[1] E. D. Donets *et al.*, At. Energ. **16**, 195 (1963).

[2] E. D. Donets *et al.*, Zh. Eksp. Teor. Fiz. **43**, 11 (1962).

[3] H. W. Gaggeler *et al.*, Nucl. Phys. A **502**, 561c (1989).

[4] R.-D. Herzberg and P. T. Greenlees, Prog. Part. Nucl. Phys. **61**, 674 (2008).

[5] G. Münzenberg, Nucl. Phys. A **944**, 5 (2015).

[6] K. Morita *et al.*, J. Phys. Soc. Jpn. **73**, 2593 (2004).

[7] K. Morita *et al.*, J. Phys. Soc. Jpn. **76**, 045001 (2007).

[8] K. Morita *et al.*, J. Phys. Soc. Jpn. **81**, 103201 (2012).

[9] Yu. Ts. Oganessian *et al.*, Nucl. Phys. A **944**, 62 (2015).

[10] Yu. Ts. Oganessian *et al.*, Phys. Rev. Lett. **109**, 162501 (2012).

[11] J. B. Roberto *et al.*, Nucl. Phys. A **944**, 99 (2015).

[12] Yu. Ts. Oganessian and K. Rykaczewski, Phys. Today **68**(8), 32 (2015).

[13] M. Bender, K. Rutz, P.G. Reinhard, J.A. Maruhn, and W. Greiner, Phys. Rev. C **60**, 034304 (1999).

[14] S. Cwiok *et al.*, Nature (London) **433**, 705 (2005).

[15] J. Dobaczewski *et al.*, Nucl. Phys. A **944**, 388 (2015).

[16] A. Karpov and V. Saiko, Phys. Part. Nucl. Lett. **16**, 667 (2019).

[17] D. C. Hoffman *et al.*, Phys. Rev. C **41**, 631 (1990).

[18] M. Leino *et al.*, Nucl. Instrum. Methods Phys. Res. B **99**, 653 (1995).

[19] P. J. Nolan, F. A. Beck, and D. Fossan, Annu. Rev. Nucl. Part. Sci. **44**, 561 (1994).

[20] R. D. Page *et al.*, Nucl. Instrum. Methods Phys. Res. B **204**, 634 (2003).

[21] B. J. P. Gall and P. T. Greenlees, Nucl. Phys. News **23**, 19 (2013).

[22] F. Khalfallah, Ph.D. thesis, Strasbourg University No. 5425, IPHC Strasbourg No. 07-010, 2007, https://inis.iaea.org/collection/NCLCollectionStore/_Public/40/010/40010115.pdf.

[23] A. G. Popeko *et al.*, Nucl. Instrum. Methods Phys. Res. B **376**, 140 (2016).

[24] A. Yeremin *et al.*, EPJ Web Conf. **86**, 0065 (2015).

[25] K. Hauschild *et al.*, Nucl. Instrum. Methods Phys. Res. A **560**, 388 (2006).

[26] A. Svirikhin *et al.*, Phys. Part. Nucl. Lett. **14**, 571 (2017).

[27] A. Lopez Martens *et al.*, Agence Nationale de la Recherche Report No.ANR-12-BS05-0013, https://anr.fr/Project-ANR-12-BS05-0013.

[28] R. Chakma *et al.*, Eur. Phys. J. A **56**, 245 (2020).

[29] A. E. Stuchbery *et al.*, Nucl. Phys. A **641**, 401 (1998).

[30] A. E. Stuchbery *et al.*, Nucl. Phys. A **548**, 159 (1992).

[31] H. Bartsch *et al.*, Nucl. Instrum. Methods **121**, 185 (1974).

[32] A. Lopez-Martens *et al.*, Eur. Phys. J. A **32**, 245 (2007).

[33] K. Hauschild *et al.*, Phys. Rev. C **78**, 021302(R) (2008).

[34] P. Mosat *et al.*, Phys. Rev. C **101**, 034310 (2020).

[35] W. J. Huang and G. Audi, EPJ Web Conf. **146**, 10007 (2017).

[36] M. Asai *et al.*, Japan Atomic Energy Agency Reprot No. JAEA-Review 2016-025, 2016 (to be published), pp. 9–10, https://jopss.jaea.go.jp/pdfdata/JAEA-Review-2016-025.pdf.

[37] G. D. Jones, Nucl. Instrum. Methods Phys. Res. A **488**, 471 (2002).

[38] K. H. Schmidt *et al.*, Z. Phys A **316**, 19 (1984).

[39] G. Duchêne *et al.*, Nucl. Instrum. Methods Phys. Res. A **432**, 90 (1999).

[40] J. Rubert, Ph.D. thesis, Strasbourg University No. 1961, IPHC Strasbourg, 2013, https://tel.archives-ouvertes.fr/tel-01260960/.

[41] M. Asai *et al.*, Nucl. Phys. A **944**, 308 (2015).

[42] C. J. Gallagher, Phys. Rev. **126**, 1525 (1962).

[43] C. J. Gallagher and S. A. Moszkowski, Phys. Rev. **111**, 1282 (1958).

[44] S. K. Tandel *et al.*, Phys. Rev. Lett. **97**, 082502 (2006).

[45] R. D. Herzberg *et al.*, Nature (London) **442**, 896 (2006).

[46] R. M. Clark *et al.*, Phys. Lett. B **690**, 19 (2010).

[47] F. P. Heßberger *et al.*, Eur. Phys. J. A **43**, 55 (2010).

[48] K. E. G. Löbner, Phys. Lett. B **26**, 369 (1968).

[49] J. M. Blatt and V. F. Weisskopf, *Theoretical Nuclear Physics* (John Wiley and Sons, New York, 1952), p. 627.

[50] F. G. Kondev, G. D. Dracoulis, and T. Kibédi, At. Data Nucl. Data Tables **103-104**, 50 (2015).